Elastic anomalies associated with transformation sequences in perovskites: II. The strontium zirconate–titanate $Sr(Zr,Ti)O_3$ solid solution series

2009 J. Phys.: Condens. Matter 21 015902

(http://iopscience.iop.org/0953-8984/21/1/015902)

J. Phys.: Condens. Matter **21** (2009) 015902 (12pp) doi:10.1088/0953-8984/21/1/015902

Elastic anomalies associated with transformation sequences in perovskites: II. The strontium zirconate–titanate $Sr(Zr,Ti)O_3$ solid solution series

Ruth E A McKnight[1], B J Kennedy[2], Q Zhou[2] and M A Carpenter[1]

[1] Department of Earth Sciences, University of Cambridge, Downing Street, Cambridge, CB2 3EQ, UK
[2] School of Chemistry, The University of Sydney, NSW, 2006, Australia

E-mail: ream3@cam.ac.uk

Received 22 August 2008, in final form 13 October 2008
Published 1 December 2008
Online at stacks.iop.org/JPhysCM/21/015902

Abstract

The sequence of phase transitions due to octahedral tilting across the $Sr(Zr,Ti)O_3$ solid solution series has been investigated by resonant ultrasound spectroscopy at high and low temperatures using ceramic samples. The elastic behaviour associated with phase transitions as a function of composition in $Sr(Zr,Ti)O_3$ at room temperature is proposed to be analogous to that as a function of temperature in $SrZrO_3$, with the $Pnma \leftrightarrow Imma$ transition at $SrZr_{0.57}Ti_{0.43}O_3$, $Imma \leftrightarrow I4/mcm$ at $SrZr_{0.35}Ti_{0.65}O_3$, and $I4/mcm \leftrightarrow Pm\bar{3}m$ at $SrZr_{0.05}Ti_{0.95}O_3$. Changes in elastic constants and acoustic dissipation with temperature have been analysed for samples across the compositional range. The intermediate phases, $I4/mcm$ and what is assumed to be $Imma$, appear to have stability fields across the full compositional range and both show large dissipation effects, most probably due to twin wall mobility. In contrast, the Zr-rich $Pnma$ phase, which should contain transformation twin walls, is an unexpectedly stiff and non-dissipating material, similar to the high temperature and/or Ti-rich $Pm\bar{3}m$ phase. In the case of $Pnma$, this is attributed to coupling between the two order parameters, which could impede relaxation responses to an applied stress. The $Pm\bar{3}m$ structure is a classically stiff cubic perovskite and no transformation-related dissipation processes are expected.

1. Introduction

Perovskites (ABO_3), in addition to undergoing temperature-dependent phase transitions, very often exhibit composition-dependent transitions at constant temperature and/or pressure. These transitions occur when there is substitution of a different cation onto the A- and/or B-site. For example, in the $(Ca,Sr)TiO_3$ system transition temperatures are lowered by substitution of Ca with Sr so that orthorhombic, tetragonal and cubic crystals can be stable at room temperature (Ball *et al* 1998, Qin *et al* 2000, Ranjan and Pandey 2001, Ranjan *et al* 2001, Harrison *et al* 2003, Carpenter *et al* 2001, 2006). Thus composition has become widely identified as a key variable parameter, whether in the context of engineering PZT electroceramics to have optimal properties, or in the context of understanding the properties of $(Mg,Fe)SiO_3$ in the Earth's lower mantle.

The primary objective of the present study was to investigate the effects of both temperature and composition on the elastic anomalies which accompany phase transitions that are, in principle, due to pure octahedral tilting transitions. In the accompanying paper (McKnight *et al* 2009), the elastic behaviour due to the pure tilting sequence of displacive phase transitions as a function of temperature in $SrZrO_3$ is presented. Here, attention is switched to elastic behaviour of the $SrZrO_3$–$SrTiO_3$ solid solution series in which Ti is substituted for Zr. The work is complementary to that of Walsh *et al* (2008) on the $(Ca,Sr)TiO_3$ system although, in the present case, the cation substitution is on the B-site rather than on the A-site.

Resonant ultrasound spectroscopy (RUS) data are presented relating to the elastic anomalies and dissipation

behaviour as a function of temperature across all compositions in the solid solution in order to determine whether the transition sequence as a function of composition at constant temperature is analogous to that as a function of temperature at constant composition. In the background, also, is the analogy with similar hierarchies of phase transitions in systems such as $BaTiO_3$ (e.g. Cheng *et al* 1994, Zhang *et al* 1994), in which transitions are driven by ferroelectric displacements rather than octahedral tilting.

$(Ca,Sr)TiO_3$ is a displacive system with a characteristic hierarchy of transitions, $Pm\bar{3}m \leftrightarrow I4/mcm \leftrightarrow Pnma$, due to octahedral tilting. The $Sr(Zr,Ti)O_3$ system is of additional interest as there is an intermediate phase, $Imma$, known to occur in $SrZrO_3$ (Howard *et al* 2000) which is not observed in $CaTiO_3$ (Carpenter *et al* 2006). The $SrZrO_3$ and $SrTiO_3$ end members have also been well characterized by diffraction methods, and there is therefore good structural information against which an interpretation of the elastic behaviour can be set. $SrZrO_3$ undergoes a sequence of transitions as a function of temperature, from the parent cubic $Pm\bar{3}m$ phase, through tetragonal $I4/mcm$ and orthorhombic $Imma$ phases, to the orthorhombic $Pnma$ phase at room temperature (Kennedy *et al* 1999, Howard *et al* 2000). The $SrTiO_3$ end member is well known to be cubic $Pm\bar{3}m$ down to ~106 K, where it transforms to tetragonal $I4/mcm$ (e.g. Hayward and Salje 1999).

Although $SrZrO_3$ and $SrTiO_3$ have been characterized in some detail, little is known about their solid solution and transitions as a function of composition. Wong *et al* (2001) carried out an investigation across the compositional range using neutron and synchrotron diffraction. A transition from orthorhombic to tetragonal symmetry at approximately $SrZr_{0.6}Ti_{0.4}O_3$ was determined using the presence of weak superlattice reflections in the x-ray powder diffraction profiles. The 021 and 122/212 reflections, near $2\theta = 33°$ and 41° (Cu Kα radiation) or 17.0° and 21.5° (synchrotron radiation, wavelength 0.8 Å), which Wong *et al* (2001) suggest are 'indicative of orthorhombic symmetry', are observed only in compositions with less than 40 mol% $SrTiO_3$. Above 40% $SrTiO_3$ content, the structure determined from neutron diffraction profiles was refined to be tetragonal in $I4/mcm$. There is then a transition from tetragonal to cubic at approximately $SrZr_{0.05}Ti_{0.95}O_3$. This was determined based on the disappearance of the 121 reflections (at $2\theta \approx 40°$) in the neutron diffraction profiles, which Wong *et al* (2001) state 'are good indicators of tetragonal symmetry'. Peak splitting of the 202/022-type reflections was also observed in low symmetry structures, but this was not used to determine exact transition compositions as the splitting could not be resolved for any compositions with more than 20 mol% $SrTiO_3$, even using synchrotron data.

2. Experimental details

2.1. Sample synthesis

Powder samples of different compositions across the solid solution series were initially made by Wong *et al* (2001) for the purposes of neutron and x-ray diffraction experiments. Synthesis of these powders was achieved by mixing high-purity $SrCO_3$, TiO_2, and ZrO_2 in the appropriate stoichiometric ratios in an acetone slurry and grinding by hand, using an agate mortar and pestle, until dry. The homogeneous solid mixtures were then compressed in alumina crucibles and heated in air at 800 °C for 24 h, 1200 °C for 24 h, and finally 1400 °C for 96 h with periodic regrinding, mixing and pressing. The powders described by Wong *et al* (2001) and used here to prepare parallelepipeds for RUS contained 25, 45, 55, 65, 72.5, 77.5, 87.5, 90, 95, and 97.5% $SrTiO_3$. All compositions are specified below by recording their $SrTiO_3$ content in this way, though the % is dropped for convenience.

The synthesis process described by Wong *et al* (2001) was used to try and prepare samples with some other compositions (10, 20, 30, 35, 37.5, 40, 42.5 and 92.5). Characterization of the final samples by x-ray diffraction, however, revealed that the powders were two-phase mixtures of $SrZrO_3$ and $SrTiO_3$ rather than being single homogeneous phases across the solid solution. A further heat treatment involving annealing compacted pellets of each powder for 48 h at 1600 °C was found to induce complete chemical homogenization so the final process to make each of the new powder samples was as follows:

Step 1: Powder samples synthesized following the method of Wong *et al* (2001).
Step 2: Ball milled at 600 rpm for 60 min in an agate ball mill with acetone.
Step 3: Pressed into 2 pellets using approximately 5 g powder for each, under a vacuum, with ~2500 psi (≈17.2 MPa) uniaxial pressure in a bench-top press for 5 min.
Step 4: Pellets annealed in a horizontal resistance furnace with a sequence of heating and cooling stages:
(a) Heat from 20 to 1550 °C at a rate of 10 °C per minute.
(b) Dwell at 1550 °C for 2 h.
(c) Heat from 1550 to 1600 °C at a rate of 5 °C per minute.
(d) Dwell at 1600 °C for 48 h.
(e) Cool from 1600 to 20 °C at a rate of 3 °C per minute.
Step 5: Pellets ground by hand in acetone in an agate pestle and mortar until they were dry and the consistency of a smooth powder.
Step 6: Structural states of powders checked using x-ray diffraction.

All of the final homogeneous powders, i.e. those made by Wong *et al* (2001) and the rest made specifically for this study, were finally ground in a agate ball mill in acetone at 600 rpm for 60 min. Approximately 4 g of powder was used to make a pellet of each composition, which was pressed in a standard cylindrical IR pellet die (diameter 13 mm) under vacuum with a uniaxial pressure of approximately 2500 psi (≈17.2 MPa) for 5 min. The pellets were then annealed with the same heating and cooling sequence as in Step 4 above.

After annealing, several parallelepipeds with approximate dimensions of 2 mm × 3 mm × 4 mm were cut from each cylindrical pellet using a fine annular diamond saw, lubricated with paraffin. Parallelepipeds were examined under a reflected light microscope to check for visible cracks. Samples

without any obvious cracks were the ones selected for RUS experiments. Offcuts of each pellet were ground by hand in an acetone slurry, using an agate pestle and mortar, for final characterization by powder x-ray diffraction. The precise dimensions, mass and density of all samples used for RUS measurements are shown in table 1.

Parallelepipeds used for RUS had densities that were consistently greater than 92% of their theoretical densities, as determined from their edge dimensions and mass. Theoretical densities were calculated using a straight line fit (vol $= 69.19 - 9.9035x$, where x is the mole fraction of $SrTiO_3$) through the lattice parameter data of Wong *et al* (2001), fixing the intercept at the $SrZrO_3$ end at 69.19 Å, which is the primitive unit cell volume determined from the room temperature values of the reduced lattice parameters plotted in figure 3 of Howard *et al* (2000). Samples with compositions 37.5, 40, 42.5 and 92.5 were only synthesized as far as Step 4 above and it was discovered during experimentation that these had much lower densities (∼70–85% of the theoretical density). The high temperature RUS data for these samples has still been used in the following analysis, as transition temperatures and the temperature dependence of Q^{-1} should not be affected by porosity. Parallelepipeds with compositions 37.5 and 40% $SrTiO_3$ were, however, remade following the full synthesis process in order to obtain room temperature data for samples with densities greater than 92%. The synthesis routes followed for each parallelepiped used in this study are detailed in table 2.

The pure $SrZrO_3$ end member sample is described in the accompanying paper on the phase transition sequence in $SrZrO_3$ (McKnight *et al* 2009). The pure $SrTiO_3$ end member sample was the CST100/1 RUS parallelepiped used by Walsh *et al* (2008) in their study of elastic anomalies in $(Ca,Sr)TiO_3$ perovskites.

2.2. RUS data collection and analysis

RUS spectra were collected initially at room temperature for all the parallelepipeds cut for each composition. Each was measured in the frequency range 200–1200 kHz in 4 different orientations to ensure that all resonances were excited and observed.

High temperature experiments were carried out on samples with compositions 0, 10, 20, 25, 30, 35, 37.5, 40, 42.5, 45, 55, 65, 72.5, 77.5, 87.5, 90, 92.5, and 95% $SrTiO_3$. Each parallelepiped was heated from room temperature in 30 K steps to well above the point at which the cubic–tetragonal transition was expected to take place. Samples with less than 35% $SrTiO_3$ were heated to above 1450 K, compositions from 37.5 to 77.5 were heated to above 1070 K, and compositions greater than 77.5 were heated to above 685 K. All samples were then cooled in smaller steps (5–10 K) with the temperature interval decreased further (1–2 K) in the regions where transitions were expected to take place. At each temperature step, samples had an appropriate equilibration time according to the heating/cooling rate: steps of 30 K had 15–30 min for equilibration, 10 K steps had 15 min, 5 K steps had 10 min, and 1–2 K steps had 5 min. After every equilibration, a resonance spectrum was collected for frequencies in the region 200–1200 kHz with 50 000 data points. Spectra collected during cooling were used for the detailed analysis and spectra collected during heating were used simply to check for the reversibility of the transitions.

Low temperature experiments were carried out on compositions 0, 77.5, 90, 97.5, and 100. Samples were cooled in 20–40 K steps down to 10 K, except for the pure $SrZrO_3$ sample (composition 0) which was only cooled to 153 K. Spectra were collected during heating back to room temperature in 5 K steps, which were reduced to 1 K increments in the vicinity of temperatures where transitions were expected to occur. An appropriate settle time was used for each temperature step: steps of 20 K had 15 min, 5 K steps had 10 min, and 1 K steps had 5 min. Spectra were collected in the frequency region 200–1500 kHz with 50 000 data points.

The RUS apparatus used for these experiments, the calibration of high temperature data, and the methods used for analysis of the RUS spectra collected, including measuring the quality factor, Q, and determining best fits for bulk and shear moduli (K and G respectively) using the DRS software (Migliori and Sarrao 1997) are described in detail in the accompanying paper (McKnight *et al* 2009).

3. Results

3.1. Room temperature phase transitions

Peak frequencies in the initial room temperature spectra for all compositions were measured for all orientations. These values were used to obtain fits for K and G at room temperature across the solid solution series. Porosities, as a percentage for each sample, were determined by comparing actual densities to theoretical densities (table 1). Values of K and G for parallelepipeds with density >90% were then corrected using the equations of Ledbetter *et al* (1994) to estimate values for samples with 100% density. It is not reasonable to apply the same correction to values for samples with density <90%. The complete data set (corrected and uncorrected) is included in table 1 and values corrected for porosity are displayed in figure 1(a).

Typical RMS (root mean square) errors for all fits were 0.1–0.2%, which implies a very good fit (Migliori and Sarrao 1997). Uncertainties in the elastic moduli were typically ∼0.05% for G and ∼0.5% for K, except for composition 90, which was cracked and did not yield a unique fit. Similarly to what is seen in $SrZrO_3$ (McKnight *et al* 2009), values for G are much better constrained than for K. The relatively larger error in K can also be seen in the scatter of the data in figure 1(a).

Values of K and G, corrected for porosity, (figure 1(a)) display evidence of four distinct phases across the compositional range at room temperature. Their evolution as a function of composition is similar to that seen as a function of temperature in the pure end member $SrZrO_3$ (compare figure 1(a) with figure 2(c) of McKnight *et al* (2009)). Within the stability range of the *Pnma* structure, as specified by Wong *et al* (2001), K and G are more or less constant. There is a small discontinuity or change in slope of G between 42.5 and 45, which is estimated to be where the *Pnma* structure transforms

Table 1. Summary of mass, dimensions, densities and the fitted values of the bulk modulus, K, and shear modulus, G, (both uncorrected and corrected for porosity) for all parallelepipeds used in high and low temperature RUS measurements. Theoretical densities have been calculated using the relative atomic mass (RAM) and the primitive unit cell volume for each composition. The unit cell volume was determined from a straight line fit through the data of Wong *et al* (2001), which was constrained to pass through 69.19 Å for pure $SrZrO_3$ (Howard *et al* 2000).

Sample (% $SrTiO_3$)	Sample number	RAM (a.m.u.)	Cubic unit cell volume (Å^3)	Theoretical density (g cm^{-3})	Mass (g)	Edge 1 (mm)	Edge 2 (mm)	Edge 3 (mm)	Actual density (g cm^{-3})	Porosity (%)	Observed K (GPa)	Corrected K (GPa)	Observed G (GPa)	Corrected G (GPa)
0	2B	226.842	69.19	5.444 141	0.1352	1.861	2.922	4.699	5.291 084	2.8	147.5	157.37	84.52	89.26
10	3A	222.507	68.199	5.417 630	0.1214	1.905	2.911	4.266	5.131 692	5.3	136.6	154.05	81.36	90.25
20	1B	218.170	67.209	5.390 338	0.1368	1.958	2.952	4.62	5.122 890	5.0	135.6	151.93	80.19	88.42
25	2	216.003	66.714	5.376 389	0.0777	1.994	2.496	2.995	5.212 600	3.0	147	157.6	83.68	88.71
30	1B	213.835	66.219	5.362 231	0.1219	1.949	4.263	2.864	5.122 754	4.5	138.5	153.08	85.22	93.09
35	2A	211.667	65.724	5.347 859	0.1111	2.246	2.91	3.293	5.162 018	3.5	142.4	154.38	81.93	87.71
37.5	1	210.583	65.476	5.340 592	0.1053	2.195	2.602	4.961	3.716 356	30.4	45.2	—	33.39	—
37.5	1A	210.583	65.476	5.340 592	0.0948	1.866	2.847	3.594	4.965 136	7.0	130.5	153.44	75.18	86.18
40	1	209.499	65.228	5.333 269	0.1254	2.216	2.916	4.94	3.928 378	26.3	58.3	—	40.26	—
40	1A	209.499	65.228	5.333 269	0.1018	1.843	2.87	3.829	5.026 378	5.8	139.4	159.7	78.39	87.75
42.5	1	208.415	64.981	5.325 891	0.1173	2.225	2.894	4.889	3.726 056	30.0	48.2	—	32.37	—
45	1	207.331	64.733	5.318 456	0.098	1.978	2.988	3.289	5.041 448	5.2	134.3	151.75	75.13	83.12
55	3	202.995	63.743	5.288 140	0.1062	1.974	2.992	3.604	4.989 201	5.7	133.6	153.28	71.65	81.01
65	1	198.660	62.752	5.256 867	0.1117	1.963	2.976	3.947	4.844 319	7.8	121	146.46	63.53	73.87
72.5	1	195.408	62.009	5.232 756	0.116	3.025	3.985	1.988	4.840 474	7.5	126	152.19	63.2	73.02
77.5	3	193.241	61.514	5.216 359	0.1177	2.024	2.998	3.963	4.894 521	6.2	132.5	154.29	69	77.78
87.5	1	188.905	60.524	5.182 760	0.0983	2.007	2.985	3.388	4.843 044	6.6	135.6	158.58	74.85	85.09
90	1A	187.821	60.277	5.174 187	0.1108	1.983	2.975	4.019	4.673 175	9.7	Cracked	Cracked	Cracked	Cracked
92.5	1	186.737	60.029	5.165 545	0.1384	2.211	2.927	4.902	4.362 659	15.5	109.5	—	65.21	—
95	1A	185.653	59.782	5.156 830	0.0363	1.303	1.973	2.969	4.755 815	7.8	139.5	164.56	94.14	109.89
97.5	1A	184.569	59.534	5.148 043	0.1117	1.984	2.991	3.985	4.723 531	8.2	143.3	170.42	97.12	114.28
100	1	183.485	59.287	5.139 183	0.0968	4.782	2.426	1.764	4.730 166	8.0	144.3	170.49	100.3	117.6

Table 2. Synthesis routes, frequencies of resonance peaks that were analysed in detail, and estimated transition temperatures for each parallelepiped used in RUS measurements. Corrected transition temperatures are calculated using the calibration described in McKnight *et al* (2009). All samples synthesized from the powders made by Wong *et al* (2001) were annealed only once and pellets were made directly from the powders. 'Double annealing' refers to the process described in the text, involving a second heat treatment. $T1$ is the $Pnma \leftrightarrow Imma(?)$ transition, $T2$ is $Imma(?) \leftrightarrow I4/mcm$, and $T3$ is $I4/mcm \leftrightarrow Pm\bar{3}m$.

Sample (% $SrTiO_3$)	Sample number	Powder made by	Pellet synthesis from powder	Room T frequency of peak analysed (Hz)	Observed $T1$ (K)	Corrected $T1$ (K)	Observed $T2$ (K)	Corrected $T2$ (K)	Observed $T3$ (K)	Corrected $T3$ (K)
0	2B	Aldrich	Single annealing	481 852	1048	1037.75	1133	1121.56	1382	1367.08
10	3A	THIS STUDY	Double annealing	458 506	948	939.143	1119	1107.76	1300	1286.23
20	1B	THIS STUDY	Double annealing	491 424	828	820.818	1125	1113.67	1210	1197.49
25	2	Wong *et al* (2001)	Single annealing	584 549	773	766.586	968	958.863	1163	1151.14
30	1B	THIS STUDY	Double annealing	279 168	681	675.87	848	840.539	1080	1069.3
35	2A	THIS STUDY	Double annealing	520 283	600	596.001	750	743.907	1073	1062.4
37.5	1	THIS STUDY	Single annealing	272 060	512	509.229	711	705.451	1043	1032.82
37.5	1A	THIS STUDY	Double annealing	None	—	—	—	—	—	—
40	1	THIS STUDY	Single annealing	284 525	460	457.955	680	674.884	1003	993.375
40	1A	THIS STUDY	Double annealing	None	—	—	—	—	—	—
42.5	1	THIS STUDY	Single annealing	490 495	352	351.463	630	625.582	988	978.584
45	1	Wong *et al* (2001)	Single annealing	468 160	—	—	587	583.182	969	959.849
55	3	Wong *et al* (2001)	Single annealing	423 282	—	—	440	438.234	860	852.371
65	1	Wong *et al* (2001)	Single annealing	368 697	—	—	318	317.937	738	732.074
72.5	1	Wong *et al* (2001)	Single annealing	372 133	—	—	—	—	653	648.261
77.5	3	Wong *et al* (2001)	Single annealing	494 704	—	—	217	217	593	589.098
87.5	1	Wong *et al* (2001)	Single annealing	470 226	—	—	—	—	400	398.793
90	1A	Wong *et al* (2001)	Single annealing	674 027	—	—	132	132	346	345.546
92.5	1	THIS STUDY	Single annealing	434 290	—	—	—	—	333	332.728
95	1A	Wong *et al* (2001)	Single annealing	623 437	—	—	—	—	273	273
97.5	1A	Wong *et al* (2001)	Single annealing	1458 700	—	—	81	81	194	194
100	1	Walsh *et al* (2008)	Walsh *et al* (2008)	492 650	—	—	—	—	106	106

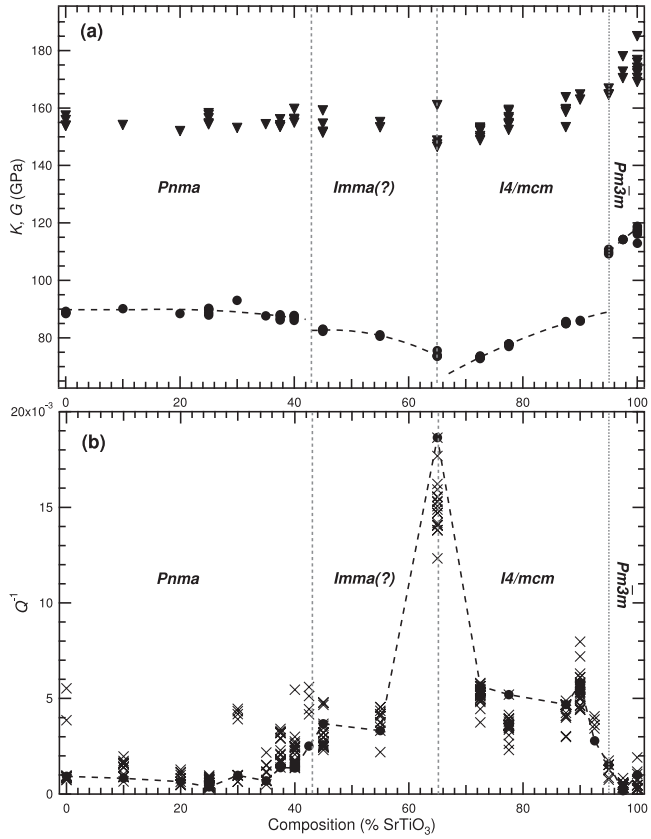

Figure 1. Room temperature values of bulk and shear moduli, K and G, corrected for porosity (triangles and circles respectively) and the inverse quality factor, Q^{-1}, (crosses) across the $SrZrO_3$–$SrTiO_3$ solid solution series. Dashed lines through the data for G in (a) are guides to the eye. Multiple values of Q^{-1} in (b) represent repeated measurements on two or more parallelepipeds of each composition. The dashed line joining the filled circles in (b) follows the evolution of Q^{-1} for all compositions measured using the high temperature RUS head after heating and cooling cycles, except for compositions 97.5 and 100 which were measured on the low temperature RUS head after cooling and reheating. Compositions at which changes in structure are interpreted to occur are marked in both (a) and (b) as dotted lines and the supposed space groups of each phase are labelled.

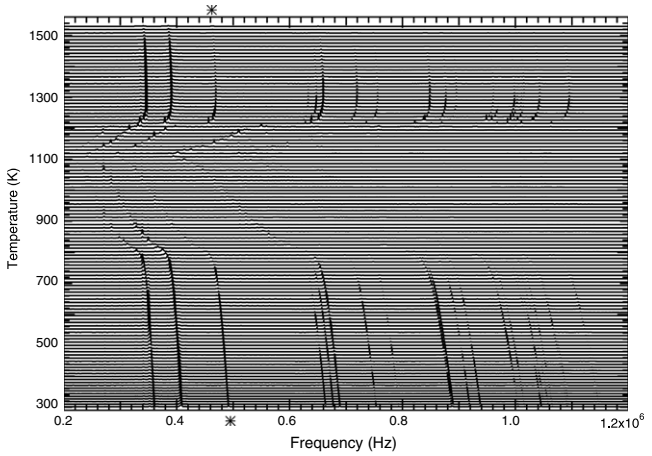

Figure 2. Stack of RUS spectra for the parallelepiped with composition 20, collected in the frequency range 200–1200 kHz during cooling from 1531 K to room temperature. In this plot the y-axis is amplitude but the spectra have been displaced in proportion to the temperature at which they were collected. This temperature scale is then shown as the y-axis. This composition is representative of all compositions between 0 and 42.5, which are $Pnma$ at room temperature (figure 1(a)) and show three high temperature structural phase transitions (figure 6). The highest temperature transition ($Pm\bar{3}m \leftrightarrow I4/mcm$ at 1198 K) is marked by a sudden decrease in peak frequencies with a change in slope at the transition. The intermediate transition ($I4/mcm \leftrightarrow Imma(?)$ at 1114 K) shows a dip in frequencies with the minimum at the transition temperature. The frequency evolution at the lowest temperature transition ($Imma(?) \leftrightarrow Pnma$ at 821 K) is virtually a mirror image of the behaviour at the highest temperature transition. Asterisks mark the single resonance peak that was measured across the full temperature range in order to analyse frequency and Q^{-1} evolution (figure 6). This peak is representative of all other peaks at this composition.

to a higher symmetry phase. This is approximately the same composition at which Wong *et al* (2001) observed the reflections 'indicative of orthorhombic symmetry' to disappear from synchrotron diffraction profiles. There is a noticeable softening (decrease) of ∼15 GPa in G (and probably also in K) between compositions 45 and 65. Between 65 and 72.5, the evolution of the elastic moduli is consistent with a similar dip to that seen in pure $SrZrO_3$, where the $Imma \leftrightarrow I4/mcm$ transition occurs. There is a stiffening (increase) of ∼20 GPa in G from 72.5 to 90 and then an abrupt discontinuity between 90 and 95, at which point the $I4/mcm \leftrightarrow Pm\bar{3}m$ transition is assumed to occur. This is also the composition at which Wong *et al* (2001) reported seeing reflections which 'are good indicators of tetragonal symmetry' disappear. In the compositional region between 95 and 100, the moduli are much stiffer (i.e. larger) than for all other phases (by up to 40 GPa) and G of the $Pnma$ phase is noticeably stiffer than for either of the two intermediate phases (by up to 20 GPa).

Dissipation behaviour across the solid solution series, as shown by the inverse quality factor, Q^{-1}, is displayed in figure 1(b). These data also show evidence for the three phase transitions at compositions of approximately 43, 65 and 95. Q^{-1} is low (∼0.001) in the $Pnma$ phase between 0 and 37.5, at which point it starts to increase. This corresponds with the composition at which a slight softening in K and G starts to occur (figure 1(a)). In the compositional range 43–95, Q^{-1} is high (∼0.003–0.007), with a significant scatter in values. There is a marked peak at composition 65, where Q^{-1} reaches ∼0.019 and there is a corresponding dip in K and G. The Ti-rich $Pm\bar{3}m$ phase shows very low Q^{-1} (∼0.001) similar to the Zr-rich $Pnma$ phase. Comparison of these results with the temperature-dependent Q^{-1} behaviour of $SrZrO_3$ (compare figure 1(b) with figure 2(b) of McKnight *et al* (2009)) shows that the patterns of dissipation are quite similar. Particularly of note is that, in the $Pnma$ phase, as temperature increases in $SrZrO_3$ or as Ti content increases across the solid solution series, Q^{-1} starts to increase in the same way ahead of the first transition. Also, dissipation is significantly higher across the two intermediate phases, both as a function of temperature and composition, and in both cases the $Pm\bar{3}m$ phase returns to very low Q^{-1}.

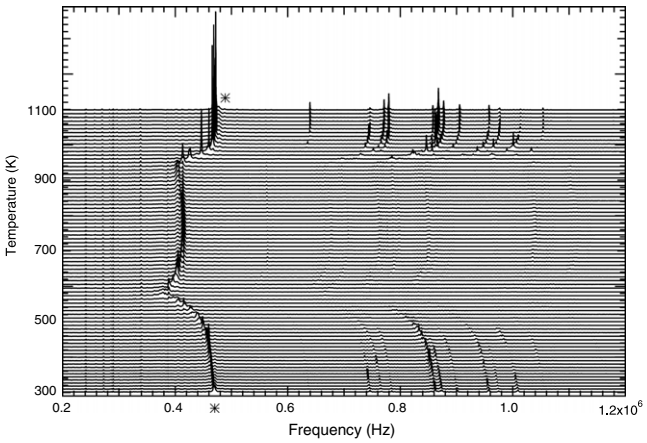

Figure 3. Stack of RUS spectra for the parallelepiped with composition 45, collected in the frequency range 200–1200 kHz during cooling from 1099 K to room temperature. The y-axis is the same as for figure 2. At this composition, the lowest temperature transition ($Imma(?) \leftrightarrow Pnma$) seen in figure 2 is no longer observed and this composition has the structure of the intermediate phase ($Imma(?)$) at room temperature. Asterisks mark the single resonance peak that was measured across the full temperature range in order to analyse frequency and Q^{-1} evolution (figure 6). This peak is representative of all other peaks at this composition. This stack of spectra is representative of the behaviour of all compositions between 45 and 92.5 which show a very similar evolution of frequencies on cooling, with two phase transitions as a function of temperature (figure 6).

3.2. Phase transitions as a function of temperature

Figures 2–5 display a selection of the raw RUS data collected for individual compositions as a function of temperature. All high temperature data has been corrected according to the calibration described in McKnight *et al* 2009. The stacks show clearly how resonance peaks change frequency with temperature, and there are obvious abrupt changes in slope of the frequency evolution, which are interpreted as being due to phase transitions. The square of the frequency of each mode is known to be directly proportional to the elastic constant(s) associated with that mode (Migliori and Sarrao 1997). Most of the resonances are dominated by shear and, therefore, the raw data essentially reveal the form of G as a function of temperature. Similarly, line broadening immediately reveals the pattern of dissipation. In some cases, the dissipation is so significant that the peaks disappear, especially in the two intermediate phases, though their frequencies can be followed approximately in most cases due to amplification of instrument noise (as explained in McKnight *et al* (2009)). Figure 6(a) includes the frequency evolution of an individual peak in each set of spectra at all compositions shown as a function of temperature. The associated behaviour of dissipation, Q^{-1}, with temperature is stacked as a function of composition in figure 6(b). Room temperature frequencies of the peak measured for each composition are listed in table 2, and these peaks are starred in the RUS stacks in figures 2–5.

The evolution of frequencies for composition 20 (figure 2) shows the same pattern of three transitions as a function of temperature as is observed in pure $SrZrO_3$ and also as a function of composition at room temperature for the solid solution series. At 1198 K, there is a change in slope accompanied by an increase in dissipation that represents the $Pm\bar{3}m \leftrightarrow I4/mcm$ transition. The dip in frequencies at 1114 K marks the intermediate transition. In this region, dissipation is high, and it is therefore difficult to observe the transition using the Q^{-1} data. The change in slope of frequency along with a decrease in dissipation associated with the transition to $Pnma$ is at 821 K. All compositions between 0 and 42.5 show a similar pattern of frequency and Q^{-1} evolution above room temperature, as can be seen in the data for individual peaks plotted in figures 6(a) and (b) respectively. Transition temperatures have all been estimated for these compositions by following the changes in slope of frequency evolution and the associated changes in Q^{-1} from $SrZrO_3$, where the transition temperatures are known independently, to progressively $SrTiO_3$ richer compositions. The temperatures of the intermediate transition are estimated only from the dip in frequencies. As dissipation is relatively high in this region and peaks are difficult to distinguish from instrument noise, the dip is most easily seen if one views the RUS stacks almost horizontally along the page.

RUS spectra for composition 45 (figure 3) show the $Pm\bar{3}m \leftrightarrow I4/mcm$ transition at 960 K, and the second transition at 583 K. For this composition, the change in slope and sudden change in Q^{-1} associated with the transition to $Pnma$ is no longer observed. This interpretation matches the suggestion of Wong *et al* (2001), that this transition occurs above room temperature only in $SrZrO_3$-rich compositions, though their estimate was that the room temperature transition occurs at composition 40. It has been concluded here, on the basis mainly of the evolution of Q^{-1} (figure 6(b)) that compositions 40 and 42.5 also undergo this transition above room temperature. The boundary between $Pnma$ and $Imma(?)$ fields is hence placed here between 42.5 and 45. Compositions 55 and 65 show exactly the same pattern of elastic anomalies, but it appears that composition 65 undergoes the intermediate transition with the dip in frequencies just above room temperature (318 K). This transition was not observed in high temperature spectra at the next composition (72.5), and it is concluded that the room temperature transition between intermediate phases, which was not observed in the study by Wong *et al* (2001), is at a composition close to but just above 65.

RUS spectra for the next composition, 77.5, were measured at both high and low temperatures (figure 4). Changes in the spectra are consistent with the same two transitions seen in composition 45 (figure 3). The first transition, $Pm\bar{3}m \leftrightarrow I4/mcm$, is at 589 K and the second, $I4/mcm \leftrightarrow Imma(?)$, is at 217 K. It is not possible to transfer a parallelepiped between high and low temperature RUS heads without changing its orientation arbitrarily. As a result, resonate peaks have different amplitudes in the two sets of spectra (both are presented as one continuous stack in figure 4). This orientational effect, however, has no significant effect on the measured values of peak frequency or Q^{-1}.

Samples 87.5, 90 and 92.5 all show the $Pm\bar{3}m$ transition above room temperature, as can be seen in figure 6(a).

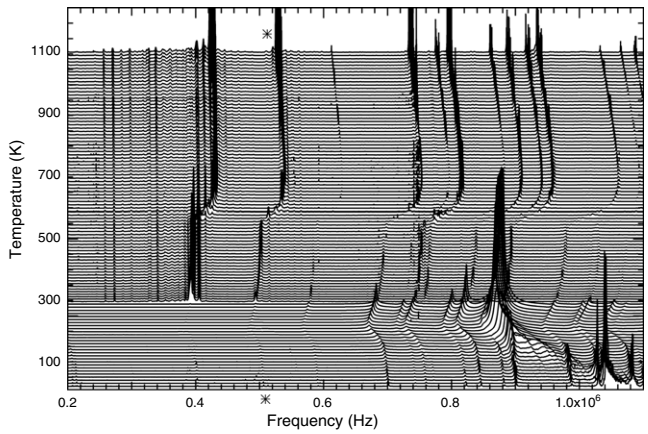

Figure 4. Stack of RUS spectra for the parallelepiped with composition 77.5, collected in the frequency range 200–1100 kHz during cooling in the furnace from 1105 K to room temperature, and then in the cryostat from room temperature to 20 K. The y-axis is the same as for figure 2. The sequence of phase transitions and frequency evolution are the same as for composition 45, except that this sample has the $I4/mcm \leftrightarrow Imma$(?) transition below room temperature. Note that the apparent change in spectra at ∼300 K corresponds to the changeover from high temperature to low temperature instruments and thus a change in sample orientation. Differences in peak heights are due simply to the acoustic resonances being excited to different extents. Asterisks mark the single resonance peak that was measured across the full temperature range in order to analyse frequency and Q^{-1} evolution (figure 6). This peak is representative of all other peaks at this composition.

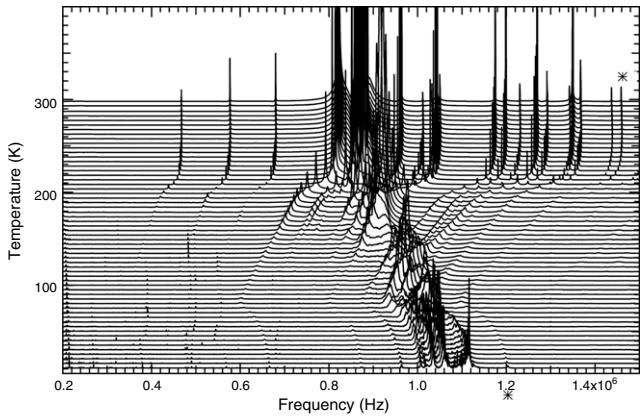

Figure 5. Stack of RUS spectra for the parallelepiped with composition 97.5, collected in the frequency range 200–1500 kHz during heating from 10 K to room temperature. The y-axis is the same as for figure 2. This composition is cubic at room temperature and shows evidence for two phase transitions. The pattern of evolution of frequencies is similar to that shown through the two high temperature transitions seen in figures 2–4. However, there is a significant decrease in frequencies on cooling across the stability field of the intermediate phase for this composition. Asterisks mark the single resonance peak that was measured across the full temperature range in order to analyse frequency and Q^{-1} evolution (figure 6). This peak is representative of all other peaks at this composition.

One effect that is noticeable in the more $SrTiO_3$-rich end of the solid solution series is that the frequency changes across this transition are more gradual. The sharp change in slope of frequency seen in the $SrZrO_3$ end member and in Zr-rich compositions is no longer observed and softening occurs over a larger temperature range (up to ∼100 K). This makes the exact temperature for this transition difficult to determine by simply looking at the frequency data. At the Ti-rich end of the solid solution series, therefore, the $Pm\bar{3}m \leftrightarrow I4/mcm$ transition temperatures are assigned to the temperature at which there is a sudden increase in Q^{-1} on cooling (see figure 6(b)). Composition 95 appears to undergo this transition at approximately room temperature. This is the same composition at which Wong *et al* (2001) also determined the $Pm\bar{3}m \leftrightarrow I4/mcm$ transition to occur at room temperature.

RUS spectra were collected below room temperature for compositions 90 and 97.5. Both show distinct softening across the stability field of the intermediate phase on cooling, as illustrated for composition 97.5 in figure 5. Again, evidence for two phase transitions can clearly be observed. Although the changes in slope of frequency evolution are not well defined, they are still visible, and the transitions for composition 97.5 are estimated to be at 194 K ($Pm\bar{3}m \leftrightarrow I4/mcm$) and 81 K ($I4/mcm \leftrightarrow Imma$(?)). In the intermediate phase between the two transitions, the peak analysed for composition 90 softens by ∼100 kHz, and the peak analysed for 97.5 softens much more by ∼300 kHz. This softening may also be seen in compositions 0, 10, 20 and 25, and in the room temperature data (figure 1(b)) as the $SrZrO_3$ content decreases across what is believed to be the $I4/mcm$ field. All other compositions appear to have a slight hump in frequencies across this phase region, but most tend to remain relatively constant (figure 6(a)). It was noted after the high and low temperature experiments that the parallelepiped with composition 90 had a crack in it, but this appears not to have affected the form of the frequency evolution significantly.

Pure $SrTiO_3$ (composition 100) shows the expected $Pm\bar{3}m \leftrightarrow I4/mcm$ phase transition at 106 K. Below this temperature, however, dissipation is so high that peaks are not measurable. Dissipation to this extent is only seen in composition 100 of the solid solution series.

3.3. *$SrZrO_3$–$SrTiO_3$ phase diagram*

Transition temperatures estimated by linking common features of the frequency and Q^{-1} data presented in figure 6 are plotted as a function of composition to make up a possible phase diagram in figure 7. For the end member phases, the transition temperatures determined in this study using RUS techniques match well with previously published data for $SrZrO_3$ (Howard *et al* 2000) and $SrTiO_3$ (e.g. Hayward and Salje 1999). Composition limits at room temperature for the stability field of the cubic, $Pm\bar{3}m$, and orthorhombic, $Pnma$, phases also match closely with the results of Wong *et al* (2001), which are shown as crosses in figure 7. From powder diffraction data alone, it is not possible to discriminate between $Imma$ and $I4/mcm$ structures unless the distortions from cubic geometry are measurable. This means that Wong *et al* (2001) did not consider the $I4/mcm \leftrightarrow Imma$ transition, postulated here to occur between compositions 65 and 72.5. Wong *et al* (2001)

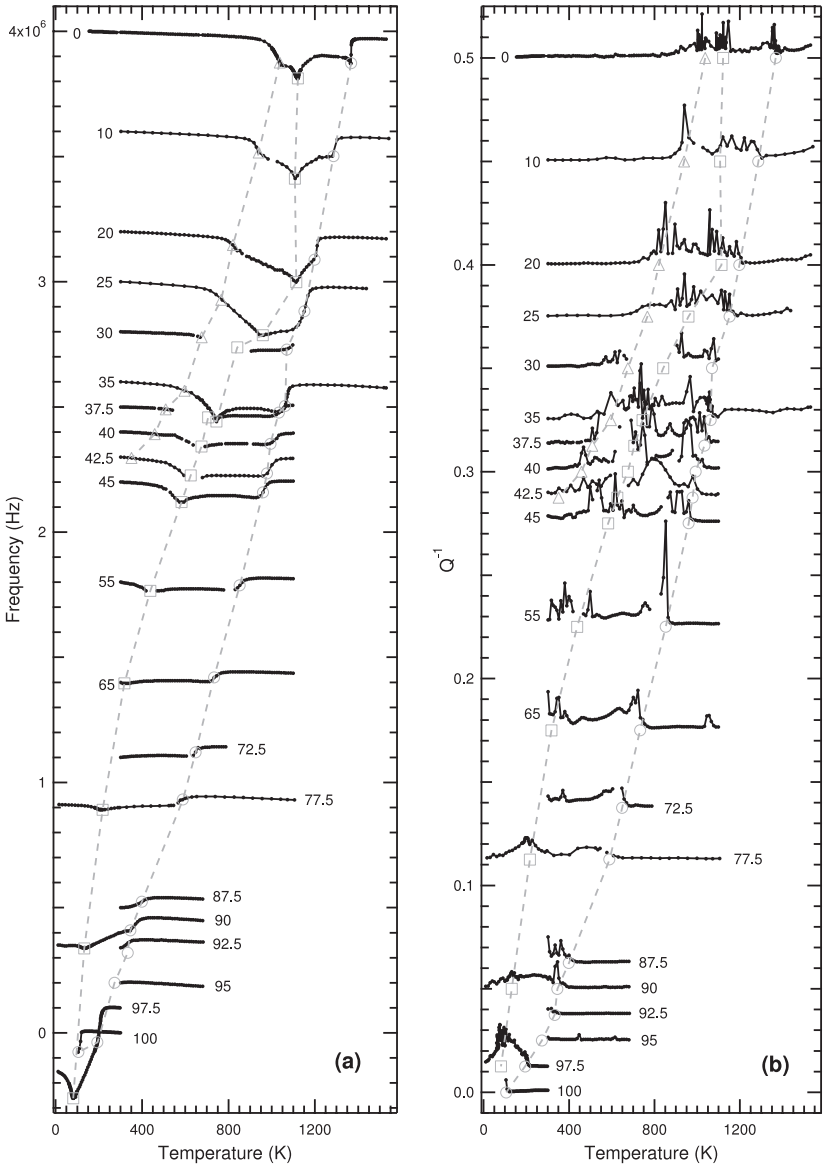

Figure 6. Frequency and Q^{-1} data for all compositions as a function of temperature. (a) shows the evolution of frequency for individual peaks with respect to temperature for each composition. For every composition, all peaks followed approximately the same form of frequency evolution; each plot is therefore representative of all resonance peaks for that particular composition. The room temperature frequencies of the individual peaks that were analysed for each composition are included in table 2. For the purposes of this figure, all frequencies were normalized to zero at room temperature by a simple subtraction; each plot has then been offset from the x-axis by an amount proportional to the composition which it represents. Similarly, (b) shows the variation of Q^{-1} with respect to temperature for each composition with each plot being representative of all peaks for that composition. Again, Q^{-1} plots are offset from the x-axis according to the composition which they represent. Compositions are marked beside each plot as mol% of Ti cations on the B-site, with 0 being $SrZrO_3$ and 100 being $SrTiO_3$. Dashed lines join similar anomalies in each data set, which are assumed to mark the phase transitions. These values are shown in table 2 as 'Corrected T_c'. Triangles represent the $Imma(?) \leftrightarrow Pnma$ $(T1)$ transition, squares are the $I4/mcm \leftrightarrow Imma(?)$ $(T2)$ transition, and circles are the $Pm\bar{3}m \leftrightarrow I4/mcm$ $(T3)$ transition.

determined transition temperatures for compositions 50 and 75, which are also shown as crosses on figure 7.

4. Discussion

4.1. Room temperature phase transitions as a function of composition

Comparison of the evolution of elastic properties as a function of composition at room temperature (figures 1(a) and (b)) with that as a function of temperature for the end member $SrZrO_3$ (McKnight *et al* 2009) appears to show similar behaviour for both. The unusually stiff *Pnma* phase that is stable up to 1038 K in $SrZrO_3$ also appears to be stable at room temperature in all compositions up to approximately 43% $SrTiO_3$. K, G and Q^{-1} are observed to have the same form as a function of composition as they do as a function of temperature, with the transition to a higher symmetry structure indicated by slight elastic softening, followed by a discontinuity in K and G and a sharp increase in dissipation.

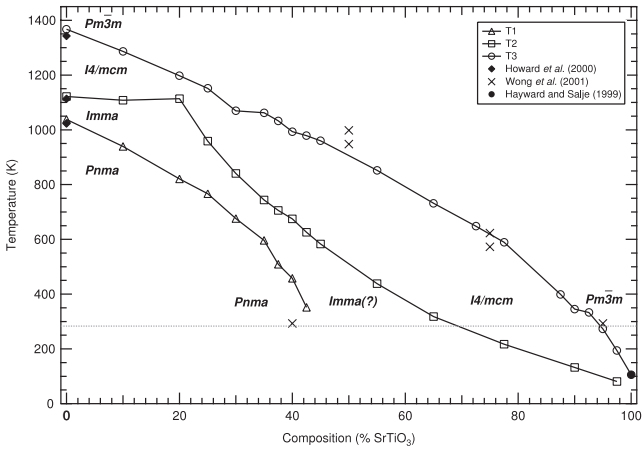

Figure 7. Temperature–composition phase diagram for the $SrZrO_3$–$SrTiO_3$ solid solution series. Open circles, squares and triangles mark the transition temperatures estimated from the data presented in figure 6. Transition temperatures for $SrZrO_3$ calculated by Howard *et al* (2000) are marked as closed diamonds. Room temperature transitions determined by Wong *et al* (2001) are marked as crosses, and the temperatures between which Wong *et al* (2001) estimated compositions 50 and 75 to undergo phase transitions are also marked as crosses. The known $SrTiO_3$ transition at 106 K (Hayward and Salje 1999) is marked as a closed circle. Space groups of each phase are labelled. Room temperature is marked as a dotted line.

Wong *et al* (2001) assumed, due to the disappearance of the reflections 'indicative of orthorhombic symmetry', that this is the $Pnma \leftrightarrow I4/mcm$ transition. However, the frequency data in figure 6 show that the pattern of evolution for $SrZrO_3$-rich compositions is closely similar to the pattern for pure $SrZrO_3$ and, hence, that the $Imma$ stability field extends significantly across the phase diagram. The transition at 43% $SrTiO_3$ is therefore tentatively assigned to $Pnma \leftrightarrow Imma$.

The elastic behaviour of the phase which is stable at room temperature between compositions 43 and 65% $SrTiO_3$ shows very similar behaviour to the $Imma$ phase observed between 1038 K and 1122 K in $SrZrO_3$, with elastic softening across the stability field away from the $Pnma$ transition, and high Q^{-1} throughout. The variation of G through composition 65 shows the same dip in frequencies and large peak in Q^{-1} as is seen for the $Imma \leftrightarrow I4/mcm$ transition in $SrZrO_3$ at 1122 K. It therefore seems sensible to assume that this phase is indeed the $Imma$ structure. From the reflections present in x-ray diffraction patterns the intermediate phase appears at least to be one with an R-point distortion but no M-point distortion operating in the structure. High resolution powder diffraction data might allow the structure type to be confirmed more definitively.

Between compositions 65 and 95% $SrTiO_3$ the $I4/mcm$ structure is assumed to be stable, given that it has been refined as such by Wong *et al* (2001), and that it transforms to the high symmetry cubic structure with the same form as is seen in $SrZrO_3$. This phase has similarly high Q^{-1} to the intermediate phase, $Imma(?)$, discussed above, in the same way as the $Imma$ and $I4/mcm$ phases have in $SrZrO_3$, and it stiffens with increasing Ti content towards the tetragonal $\leftrightarrow$ cubic transition at composition 95. At the Ti-rich end of the solid solution series (above composition 95), the structure exhibits much greater stiffness and very low Q^{-1} just as is seen in $SrZrO_3$ above 1367 K when the $Pm\bar{3}m$ phase is stable, and also in $(Ca_{0.05}Sr_{0.95})TiO_3$ at temperatures above 240 K (Walsh *et al* 2008).

4.2. High temperature transitions in Zr-rich compositions

The anomalous behaviour at high temperatures of compositions at the Zr-rich end of the solid solution is important to note. The dip of resonance frequencies and peak in Q^{-1} as a function of temperature, which has been ascribed to the middle phase transition ($Imma(?) \leftrightarrow I4/mcm$), occurs at an almost constant temperature from the pure end member $SrZrO_3$ up to composition 20, before starting to fall off (figure 7). High temperature RUS measurements were repeated several times for samples around composition 20 to confirm that this result is reproducible. Further characterization of the high temperature structures at intermediate compositions will be necessary, to determine if this feature reflects a fundamental change in the topology of the phase diagram due, say, to some other change in structure. It can, however, be concluded from the similarity of the elastic behaviour shown by $SrZrO_3$-rich compositions to that of pure $SrZrO_3$ that the hierarchy of phase transitions seen in $SrZrO_3$, as presented by Howard *et al* (2000) and in the accompanying paper (McKnight *et al* 2009), persists across the $SrZrO_3$–$SrTiO_3$ solid solution to at least a composition with 20 mol% $SrTiO_3$.

4.3. High temperature transitions as a function of composition

Above composition 20, the continued smooth curve of the cubic $\leftrightarrow$ tetragonal phase boundary (figure 7) is consistent with the expectation that all compositions across the solid solution undergo the $Pm\bar{3}m \leftrightarrow I4/mcm$ transition. In addition, this transition is well characterized as $Pm\bar{3}m \leftrightarrow I4/mcm$ for both end member phases.

The intermediate transition for all compositions greater than 20 again shows a very regular, smooth curve in the phase diagram (figure 7). This suggests that, whether the transition is $I4/mcm \leftrightarrow Imma$ or $I4/mcm$ to another phase, it is the same transition for all compositions between 20 and 97.5. In frequency and Q^{-1} measurements (figure 6), it shows exactly the same pattern of evolution as is seen for Zr-rich compositions.

The smooth variation of the lowest temperature phase boundary suggests that the $Pnma \leftrightarrow Imma$ transition observed in $SrZrO_3$ persists for all compositions up to ~43% $SrTiO_3$ at room temperature.

4.4. Mechanical properties of the different phases

A striking feature of figure 6(b) is that anomalies in Q^{-1} are restricted to a temperature interval which appears to be bounded by the stability fields of the $Pnma$ and $Pm\bar{3}m$ phases. Dissipation behaviour at RUS frequencies is thus

clearly restricted to $I4/mcm$ and $Imma$(?) structures, with temperature being either irrelevant or only a minor factor.

Mobile defects are always a possible cause of mechanical dissipation effects and transformation twin walls, in particular, have attracted considerable attention recently in this context (e.g. Harrison and Redfern 2002, Harrison *et al* 2003, 2004b, 2004c). Mobile interfaces between coexisting phases at a first order transition can have a similar influence (e.g. Wang *et al* 2000, Zhang *et al* 1995a, 1995b, Pérez-Sáez *et al* 1998, Harrison *et al* 2004a, Sondergeld *et al* 2006). As discussed in McKnight *et al* (2009), transformation twin walls must exist in $Pnma$, $Imma$ and $I4/mcm$ structures. We can now speculate that mechanical dissipation due to transformation microstructures may be switched off simply by the development of a second order parameter. The microstructures appear to be mobile and/or other factors contribute to the dissipation in systems with one non-zero order parameter (e.g. $I4/mcm$ or $Imma$) but these contributions appear to be suppressed by coupling with a second order parameter (e.g. $Pnma$).

4.5. Comparison with the $(Ca,Sr)TiO_3$ solid solution series

There are clearly close analogies between the properties and behaviour of the $SrZrO_3$–$SrTiO_3$ solid solution and those of the $CaTiO_3$–$SrTiO_3$ solid solution. The topology of the phase diagram emerging from the present study is broadly the same as that summarized for $(Ca,Sr)TiO_3$ by Carpenter *et al* (2006). In terms of the main trends of transition temperatures and stability fields, substituting a large cation (Sr, ionic radius ≈1.44 Å) for a small cation (Ca, ≈1.34 Å) on the A-site has the same effect as substituting a small cation (Ti^{4+}, ≈0.61 Å) for a large cation (Zr^{4+}, ≈0.72 Å) on the octahedral B-site (ionic radii from Shannon 1976).

It remains to be seen whether the $Pbcm$ phase of $(Ca,Sr)TiO_3$ appears at low temperature in $Sr(Zr,Ti)O_3$ but, otherwise, the main difference between the two systems at this stage is in the appearance of the $Imma$ structure. This structure develops in other perovskites (e.g. $BaCeO_3$: Genet *et al* 1999, Knight 1994, 2001; $CaTiO_3$–$La_{2/3}TiO_3$: Zhang *et al* 2007; $SrSnO_3$: Glerup *et al* 2005, Mountstevens *et al* 2005) and probably has a stability field which is never very far from that of the $I4/mcm$ or $R\bar{3}c$ structures.

It is interesting to note that the possible $I4/mcm \leftrightarrow Imma$ transition shown in figure 7 would extrapolate to ∼60 K in pure $SrTiO_3$, almost coinciding with the temperatures at which anomalies in the elastic and piezoelectric properties appear (e.g. Scott and Ledbetter 1997, Grupp and Goldman 1997).

4.6. Conclusions

In conclusion, the present study shows that the hierarchy of octahedral tilting transitions, $Pm\bar{3}m \leftrightarrow I4/mcm \leftrightarrow Imma \leftrightarrow Pnma$, gives rise to a characteristic pattern of elastic and anelastic anomalies. Structure type is more important than temperature in determining these properties, and selection of composition would allow selection of elastic stiffness and acoustic dissipation if such effects are desirable (or undesirable) for technological applications.

Acknowledgments

REAM was supported by a studentship from the Engineering and Physical Sciences Research Council (grant no. EPSRC DTG05 10026782). The RUS equipment was built with a grant from the National Environmental Research Council of Great Britain (grant no. NER/A/S/2000/01055), which is gratefully acknowledged. BJK thanks the Australian Research Council for support (grant no. DP0877695). Discussions with Chris Howard are also much appreciated.

References

Ball C J, Begg B D, Cookson D J, Thorogood G J and Vance E R 1998 *J. Solid State Chem.* **139** 238–47
Carpenter M A, Becerro A I and Seifert F 2001 *Am. Mineral.* **86** 348–63
Carpenter M A, Howard C J, Knight K S and Zhang Z 2006 *J. Phys.: Condens. Matter* **18** 10725–49
Cheng B L, Gabbay M, Fantozzi G and Duffy W Jr 1994 *J. Alloys Compounds* **211/212** 352–5
Genet F, Loridant S, Ritter C and Lucazeau G 1999 *J. Phys. Chem. Solids* **60** 2009–21
Glerup M, Knight K S and Poulsen F W 2005 *Mater. Res. Bull.* **40** 507–20
Grupp D E and Goldman A M 1997 *Science* **276** 392–4
Harrison R J and Redfern S A T 2002 *Phys. Earth Planet. Inter.* **134** 253–72
Harrison R J, Redfern S A T and Bismayer U 2004a *Min. Mag.* **68** 839–52
Harrison R J, Redfern S A T, Buckley A and Salje E K H 2004b *J. Appl. Phys.* **95** 1706
Harrison R J, Redfern S A T and Salje E K H 2004c *Phys. Rev.* B **69** 144101
Harrison R J, Redfern S A T and Street J 2003 *Am. Mineral.* **88** 574–82
Hayward S A and Salje E K H 1999 *Phase Transit.* **68** 501–22
Howard C J, Knight K S, Kennedy B J and Kisi E H 2000 *J. Phys.: Condens. Matter* **12** L677–83
Kennedy B J, Howard C J and Chakoumakos B C 1999 *Phys. Rev.* B **59** 4023–7
Knight K S 1994 *Solid State Ion.* **74** 109–17
Knight K S 2001 *Solid State Ion.* **145** 275–94
Ledbetter H, Lei M, Hermann A and Sheng Z 1994 *Physica* C **225** 397–403
McKnight R E A, Howard C J and Carpenter M A 2009 *J. Phys.: Condens. Matter* **21** 015901
Migliori A and Sarrao J L 1997 *Resonant Ultrasound Spectroscopy: Applications to Physics, Material Measurements and Nondestructive Evaluation* (New York: Wiley)
Mountstevens E H, Redfern S A T and Attfield J P 2005 *Phys. Rev.* B **71** 220102
Pérez-Sáez R B, Rescarte V, Nó M L and San Juan J 1998 *Phys. Rev.* B **57** 5684–92
Qin S, Becerro A I, Seifert F, Gottsmann J and Jiang J 2000 *J. Mater. Chem.* **10** 1609–15
Ranjan R and Pandey D 2001 *J. Phys.: Condens. Matter* **13** 4251–66
Ranjan R, Pandey D, Schuddinck W, Richard O, De Meulenaere P, Van Landuyt J and Van Tendeloo G 2001 *J. Solid State Chem.* **162** 20–8
Scott J F and Ledbetter H 1997 *Z. Phys.* B **104** 635–9
Shannon R D 1976 *Acta Crystallogr.* A **32** 751–67
Sondergeld P, Li B, Schreuer J and Carpenter M A 2006 *J. Geophys. Res.* **111** B07202
Walsh J W, Taylor P A, Buckley A, Darling T W, Schreuer J and Carpenter M A 2008 *Phys. Earth Planet. Inter.* **167** 110–7

Wang Y N, Tian W, Huang Y N, Yan F, Shen H M, Zhu J S and Zhang Z F 2000 *Phase Transit.* **72** 57–80
Wong T K-Y, Kennedy B J, Howard C J, Hunter B A and Vogt T 2001 *J. Solid State Chem.* **156** 256–63
Zhang J X, Fung P C W and Zeng W G 1995a *Phys. Rev.* B **52** 268–77
Zhang J X, Yang Z H and Fung P C W 1995b *Phys. Rev.* B **52** 278–84
Zhang J X, Zheng W, Fung P C W and Liang K F 1994 *J. Alloys Compounds* **211/212** 378–80
Zhang Z, Lumpkin G R, Howard C J, Knight K S, Whittle K R and Osaka K 2007 *J. Solid State Chem.* **180** 1083–92